Making long-distance space travel efficient: Maximizing radiative cooling in a vacuum environment

Alex Lee

Abstract

Nuclear propulsion has become a promising technology for long distance space flight. NASA has identified nuclear thermal propulsion (NTP), using uranium fission, essential for future Mars mission. A key challenge in NTP lies in the management of the excessive heat generated by the nuclear fission. Thus, an effective radiator design to maximize the cooling through radiation is crucial, as heat convection and conduction is not possible in the vacuum. for space should maximize its heat dissipation. This study examines how the heat dissipation capacity of a ribbed radiator surface varies with different vertex angles. To test this, three aluminum model radiators each with a respective vertex angle of 0°, 20°, 40° and 60° were heated to 477.6 K in a near vacuum environment then cooled over a 55-minute period. Temperatures were recording every 10 seconds using a MLX90614 infrared sensor. These data were converted into radiant power (Watts) over time, then normalized by volume to produce W/m^3 versus time graph. The 0° radiator consistently exhibited the highest W/m^3, suggesting the optimal surface geometry for cooling. Initial hypothesis predicted the highest cooling efficiency of flat radiator surface by minimizing the reabsorption of emitted radiation. In addition, the efficiency of each radiator matched with higher surface area to volume ratios, suggesting that this metric is more important in creating efficient radiators than simply surface area.

Keywords

radiative cooling, surface geometry, spacecraft heat dissipation, vacuum environment, surface area to volume ratio

Introduction

In 2024, long-distance space travel is now a top priority for many space organizations [1]. NASA has gained a keen interest in Mars and is currently developing technologies to support a manned mission. Chief amongst these technologies is nuclear thermal propulsion. This innovative propulsion method functions by triggering fission reactions in between uranium atoms that generate large amounts of heat. A liquid propellant runs in between these heated uranium fission chambers and ignites, producing thrust. Nuclear thermal propulsion can reach temperatures close to 3000 K within the reactor and at the propellant interface [1]. With such extreme temperatures comes the need to dissipate this heat.

Radiative cooling is the only method by which a spacecraft can release heat from itself. Although modern spacecraft are equipped with complex networks of heat exchangers and various cooling methods (passive/powered) to manage internal temperatures, once heat reaches the exterior, it can only dissipate through radiation. While conduction, radiation, and convection help transfer heat within a spaceship, radiation is the only means for heat to escape from a ship in the vacuum of space. Therefore, investigations to maximize the radiative properties of spaceships are essential.

Past spacecraft relies entirely on passive systems to achieve radiation, whether it is through large panels or a more complex design. The ISS already has a sophisticated internal heat management system composed of heat exchangers, cryogenic tubing, and large radiative panels [2]. However, the ISS does not need to power its own movement except to maintain constant elevation when in orbit [3]. A ship that is constantly accelerating to facilitate large-distance space travel will be constantly or near-constantly firing some sort of thruster or rocket, which will inevitably produce heat. There is already extensive research and practical designs for the cooling of internal systems of a spacecraft. However, relatively little research has been done on the impact of geometry in radiating heat from the outside of a spacecraft into space.

On earth, many radiators often feature geometrically complex surfaces to maximize the potential surface area where convection can occur. However, in space, when radiation is the only way thermal energy can leave an object, convection and conduction are not important. The purpose of this experiment was to test the effect of angled surfaces on cooling rates, and whether angled surfaces could perform better than flat surfaces. This study investigated the dynamics between an object's ribbed surface geometry and its passive cooling efficiency [4]. Having a parallel arrangement of straight alternating ribs on the object surface lowers its cooling efficiency [4]. This is because the emissivity of a surface is equal to its absorptivity, given the radiant heat dissipation pattern and a uniform chemical composition of the object [5]. It is hypothesized that a smooth surface, with no significant angle obstructions, would have a better cooling efficiency

compared to surfaces with parallel ribs. Three rough surfaces were modeled with ribs angled at 20°, 40°, and 60° from the horizontal, respectively. After obtaining a graph for Watts per meter cubed, the results showed that the surface area to volume ratio of the object also plays a significant role in determining the cooling efficiency.

Table 1. Table 1 provides a summary of various units of measurements that were adopted in the process for the experiment and data analysis.

Terms	Units/Symbols	Definitions
Luminosity	J/s or W	A measure of energy output per second by an object in the form of Joules/second
Joules	J	Joules are used as heat energy in the context of this paper but are often defined as the energy required to apply a force of one Newton over one meter distance
Watts	W	Watts are equivalent to Joules per second and are the unit of luminosity
Amps	A	One amp represents one coulomb per second
Coulomb	C	One coulomb represents the amount of electrical charge carried by 6.24×10^{18} electrons or protons

Volts	V	A unit of measurement that represents the electrical potential difference in energy across a circuit
Resistance	Ohm (Ω)	A unit for electrical resistances. Higher Ohms means that an object is an insulator while lower Ohms indicates a conductor
Specific Heat Capacity	Joules/g*K	A unit for specific heat capacity, the amount of Joules needed to raise one gram of material by one Kelvin or Centigrade
Power Density	W/m^3	A unit that indicates how much energy each unit of volume is losing per second

Materials and Methods

Vacuum Chamber

A vacuum chamber was used to simulate the vacuum of space. The single-stage motor vacuum pump utilized to achieve said vacuum was not powerful enough to achieve any pressure lower than 0.92 inHg. The vacuum chamber was originally a smaller one made of acrylic (0.22 m x 0.16 m x 0.21 m), which faced heat issues and warped from the heat generated by the heating apparatus, causing it to explosively decompress, disabling it from sealing to create a vacuum. Thus, the vacuum chamber that was used for all current trials ended up being a steel vacuum chamber with a glass lid (12.4 in diameter, 16 in height). Three holes were drilled into the vacuum chamber. Two brass electrodes were inserted halfway into the pair of holes opposite each other and a temperature sensor was inserted into the third hole before being sealed up with high-temperature epoxy. The epoxy served two purposes. First, it did not melt in high temperature environments, maintaining the vacuum seal even as its interior heated up. Second, it electrically isolated the brass electrodes from the conductive steel chamber (Figure 3). A power supply was outside of the vacuum chamber to the brass electrodes. One wire from the positive terminal of the power supply was connected to one brass electrode and the wire from the negative terminal was connected to the other electrode. Both wires were secured to the

electrodes with nuts. The heating apparatus was then placed inside the chamber and set up according to Figure 1.

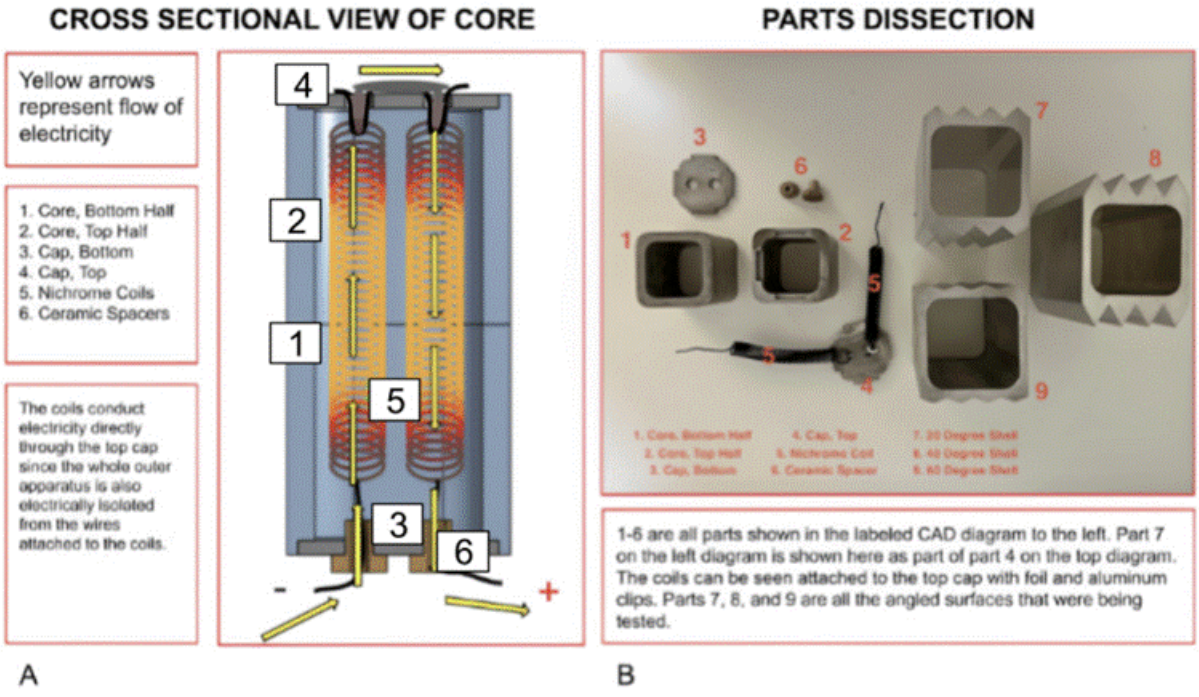

Figure 1A. Heating apparatus core diagram. The flow of electricity is shown through a cross section of the central heating device.
Figure 1B. Heating apparatus parts. All parts used to assemble the heating apparatus are shown. Each part was made using Xometry at home. No parts were pre-purchased.

Heating Apparatus

The heating apparatus was designed on Onshape, an online CAD (computer-aided design) program. The components of the heating apparatus were downloaded as .STL files, then exported and placed into Xometry, a company that allows people to place orders for parts and contracts outside fabricators to make them and ship them. The parts were then fabricated with aluminum 6061 to within a 0.002” tolerance (Figure 1). Three shells were created with ribs of 20°, 40°, or 60° from the horizontal, equivalent to 140°, 100°, or 60° for the vertex angle. The

shells fitted over an aluminum core made from two shell assemblies with end caps (Figure 1). Two nichrome coils were placed within. As the outside of the heating apparatus is electrically isolated from the rest of the wiring, it was simpler to allow the coils to conduct electricity through the top cap at one point. The ceramic spacers were secured in place by aluminum wires coiled around the nichrome section that stuck out from the apparatus. When electricity ran through the circuit, it heated up both nichrome coils. In a vacuum environment, the heat from the coils would radiate to the outer walls of the core. The core would then conduct heat to the shell placed around it. The shell would radiate this heat to the outside environment. The three shells can all be used with this aluminum core interchangeably. To heat the core sufficiently, two meters of 16-gauge nichrome wire were coiled and fitted into the four-inch tall by two-inch wide core (Figure 1).

Circuit Assembly

Due to nichrome's significantly higher resistance compared to aluminum, two kiln-fired ceramic pieces were shaped and placed over the contact points to insulate the wire to ensure that the current would flow through the nichrome instead of the aluminum shell and fail to heat the device (Figure 1). The nichrome wires were threaded through the ceramic spacers. Each wire was then connected to a piece of aluminum wire, which ran to brass electrodes. These electrodes were secured in place by high-heat epoxy, fixed through small holes in the vacuum chamber walls. The electrodes were then connected to a power supply with a maximum output capacity of 20 Amp, 60 Volt. The MLX90614 non-contact infrared temperature sensor was also positioned in the vacuum chamber through an epoxy-sealed small hole. It measured the surface temperature of the shell and was connected to an Arduino board, which was programmed to record and output the ambient temperature, object temperature, and time every ten seconds. The average error of the temperature sensor was ±0.5°C (at room temperature), and a temperature range of 70℃-382.2℃. At the end of each experimental phase, the entire device was allowed to cool off until the sensor measured the surface temperature of the aluminum heater at 26℃-27℃ and compared it with an infrared laser thermometer. The ambient temperature of the sensor was also required to match said temperature measurement. After meeting these conditions, the experiment was continued. The circuit was powered by 33 Volts, with an average resistance of 3.3Ω and minor fluctuations due to thermal noise [6]. This setup resulted in a relatively steady flow of 10 Amps of DC during the heating phase. The bottom plate upon which the whole heating apparatus and four ceramic blocks rest on top of is a simple porcelain plate. The complete setup of the apparatus is shown in Figure 2.

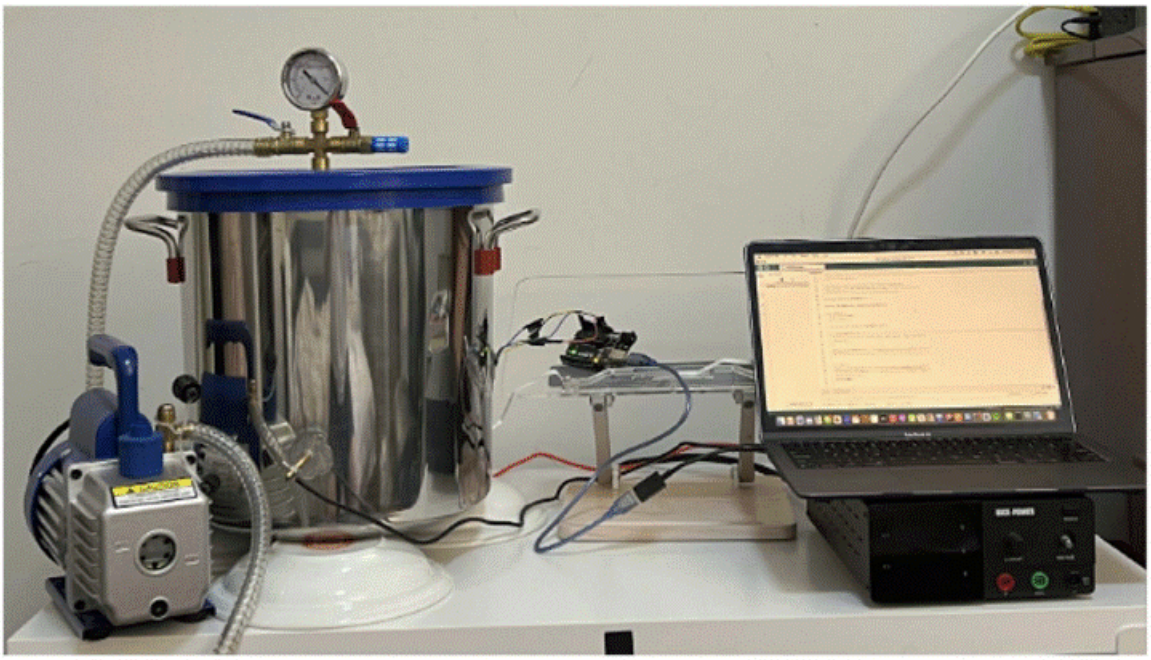

Figure 2. The final set up of the experiment. The vacuum pump is activated periodically to maintain pressure inside. The temperature within the chamber is relayed outwards by the Arduino and its infrared sensor.

Device Setup

The vacuum chamber was separated from the ground by a ceramic plate, then further separated by four kiln-fired custom-fabricated ceramic spacers. This was to prevent the bottom of the vacuum chamber from heating up to significant amounts. The apparatus was separated by a space of four inches from the walls of the chamber. The vacuum was maintained at 0.92 inHg (approximately 25 Torr), which, while lower than atmospheric pressure, does not fully replicate the ultra-low vacuum of space which reaches around 10^{-6} torr [7]. This limitation was due to the constraints of the available vacuum pump.

Running the Experiment

To run each trial, the integrity of the circuit was first tested and confirmed with 1 amp of current. After, a near vacuum was created inside the vacuum chamber. The device received slowly increasing currents, until the current reached 10 Amps. At 10 Amps, the device was heated up

to 15 Kelvin above 477.6 Kelvin, then was allowed to cool to 477.6 Kelvin upon which a 55-minute measuring phase began. During this phase, the temperature sensor registered the surface temperature of the aluminum shell's angled surface at regular ten-second intervals, producing around 330 points of data per trial. Once the device reached the end of the 55-minute period, the data were transferred into a sheet for further analysis and the power supply was shut off. After allowing air back into the chamber, the chamber underwent a further cooling phase over 20 minutes with a fan to reduce it back to ambient temperature (297.6 K). When required, the shell was swapped at the end of the extra cooling phase. If not, then the next trial was performed. Three trials were done with each shell, then three trials were performed without a shell (0°) as well. The CAD design of four shells and the vacuum chamber's internal arrangement is shown in Figure 3.

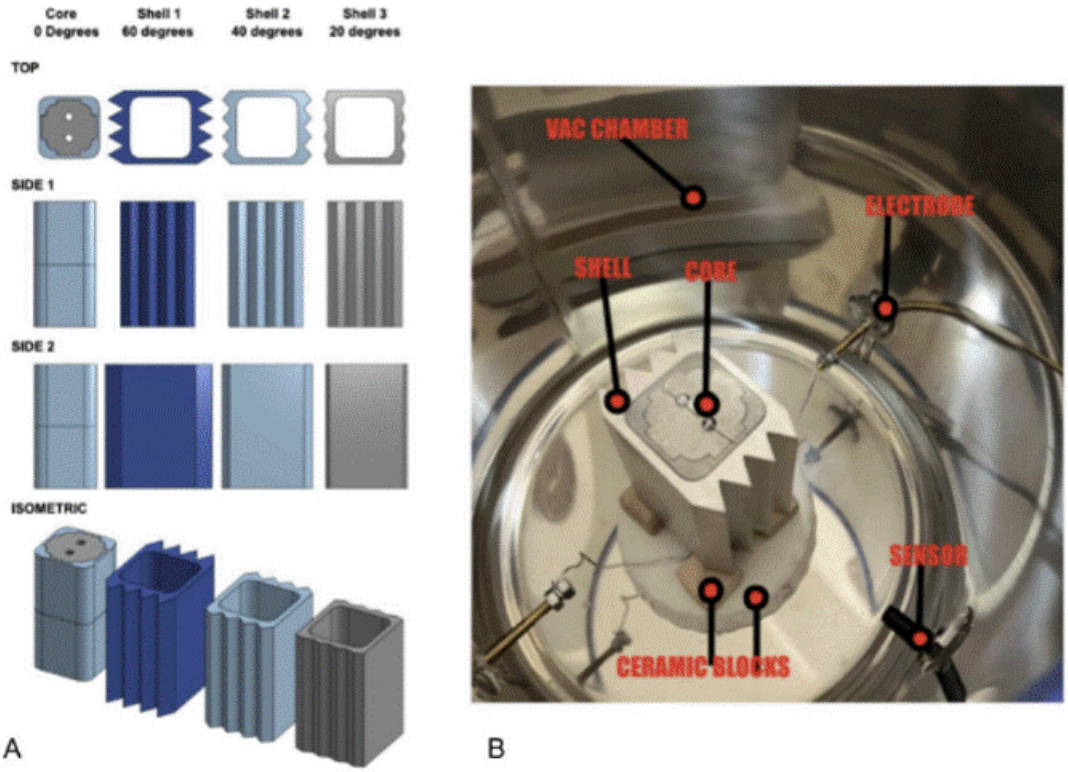

Figure 3A. Front, back, side, and isometric views of core and shell designs. These were designed in the CAD (Computer Aided Design) software, Onshape, and fabricated to a 0.002 inch tolerance using aluminum 6061. The image shown is the 60° shell.

Figure 3B. The internal workings of the vacuum chamber apparatus are shown to the right. The shell is standing on four ceramic blocks that prevent the bottom of the chamber from heating up uncontrollably. The two electrodes are also permitting the movement of electricity through the circuit from a power source outside the vacuum chamber.

Results

The 0° shell cooled down the fastest for all three trials, reaching the lowest final temperature of 344.95 K. The 40° shell was the second most efficient, the 20° trial the third most efficient, and the 60° shell reached the highest final temperature (Figure 4).

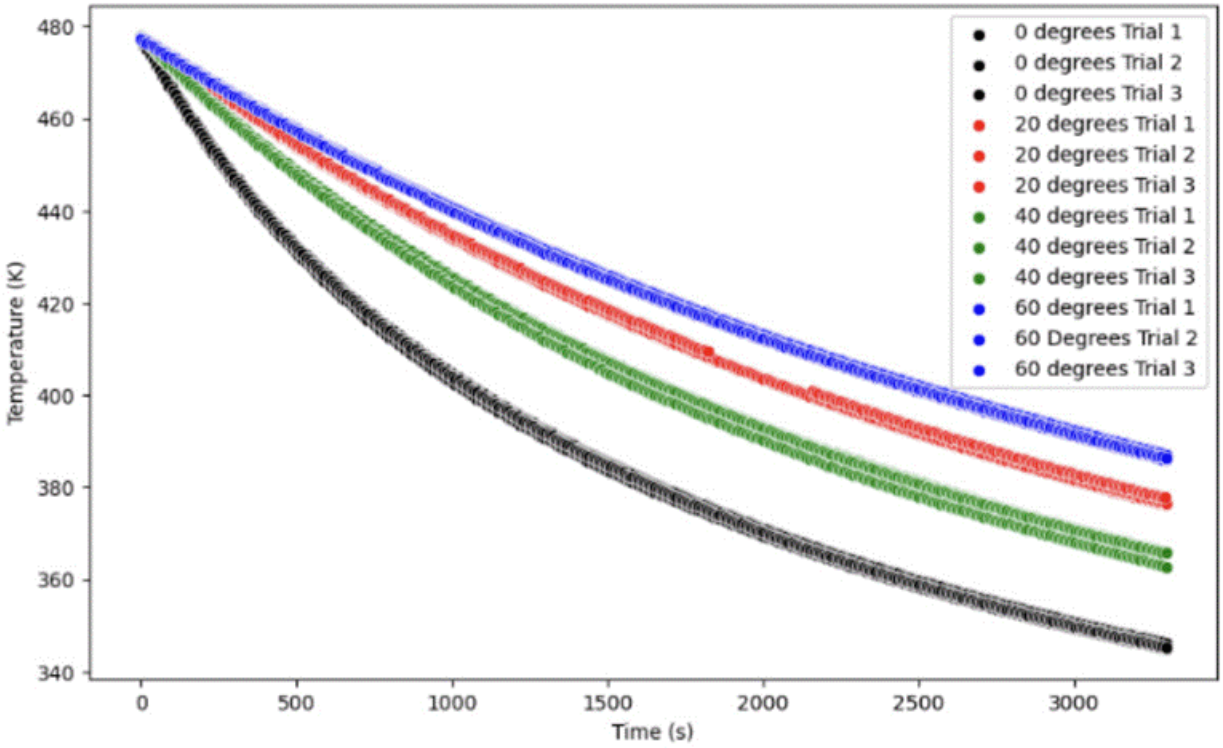

Figure 4. Raw temperature loss curves for four shells: This represents temperature (Kelvin) versus time (seconds) for all four shells. Each shell was heated to 400K and allowed to cool over 55-minute period. Three trials were performed per shell. Temporary sensor outage on “20° trial 1” is represented by the gap in data.

Then, Stefan Boltzman’s law was applied to every data point from the temperature versus time graph to obtain a luminosity versus time graph (Figure 5). Luminosity shows how many joules are being ejected per second, by the shells. In figure 5, the rate of joules released changes over time is shown.

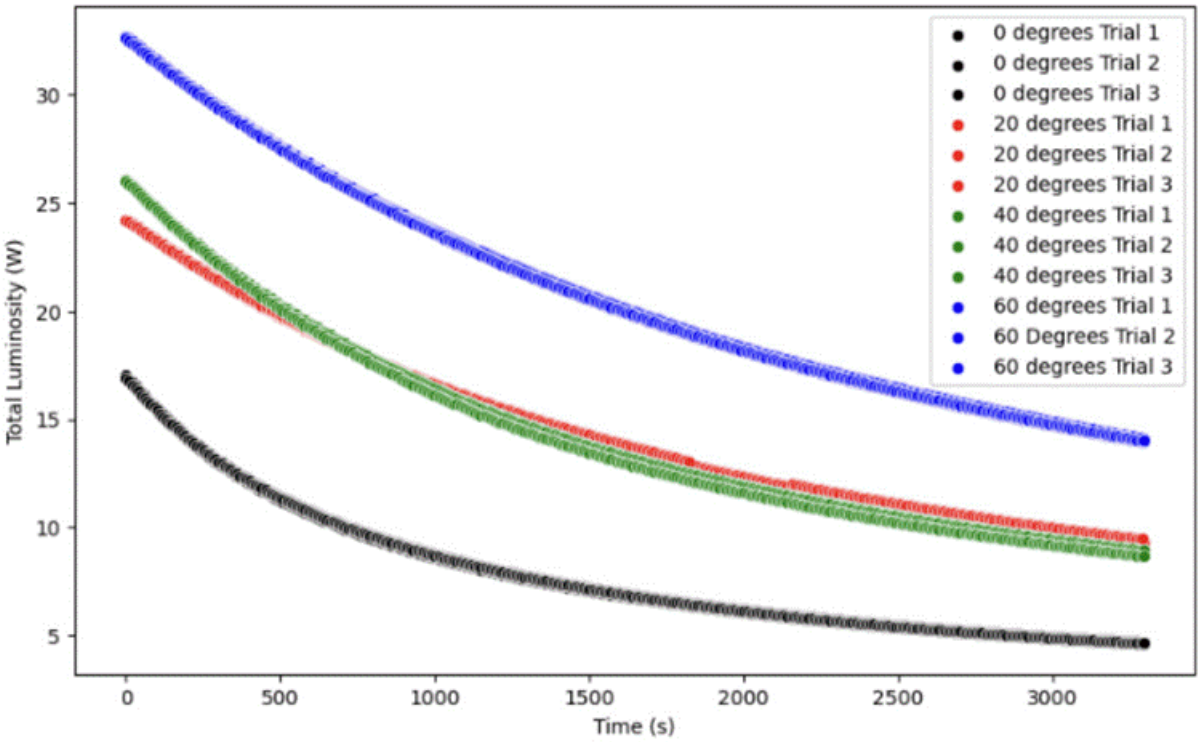

Figure 5. Total luminosity for four shells: This was a recording of the luminosity (Watts = J/s) versus time (seconds) for all four shells. Each point on the graph represents the total energy being removed per second by the entire heating apparatus for the specified shell.

The 60° shell outputted the highest luminosity for all times. This is to be expected, as all shells have the same emissivity, the 60° shell has the highest surface area, and the 60° shell consistently has the highest temperatures across all time points. The 0° shell had both the lowest surface area and lowest temperatures versus all points in time, causing its luminosity to be lower for all points in time. While the 40° shell outperformed the 20° shell in temperature over time, the 40° shell had a higher surface area, which seemed to balance out their differences, resulting in both the 20° and 40° shells having very similar luminosities versus time. While the 60° shell had the highest luminosity over time, the 60° shell cooled down the least, indicating that the shell's high volume stopped it from cooling effectively.

Calorimetry, represented by the equation (1) [8], was used to obtain the total amount of joules released from the 0° shell for all three trials then averaged this number. Then, the 0° trials from the temperature versus time graph were applied by the Stefan Boltzmann Law, represented by the equation (2), [9] to every point. However, the emissivity, ε, the emissivity of the aluminum shell is not known. To calculate this constant, the precise area was found under the curve of each of the three 0° trials (Figure 4) using Python to find the average area. The obtained

average area value was set to variable E. The Stefan Boltzman Law, where M is the Luminosity in watts, features the emissivity constant. ε is the integral of Luminosity versus time multiplied by emissivity, or the total joules released over the 55-minute period.

$$Q = mc\Delta T \quad \textbf{(1)}$$

$$M = A\varepsilon\sigma T^4 \quad \textbf{(2)}$$

$$E\varepsilon = Q \quad \textbf{(3)}$$

$$\varepsilon = (mc\Delta T)/E \quad \textbf{(4)}$$

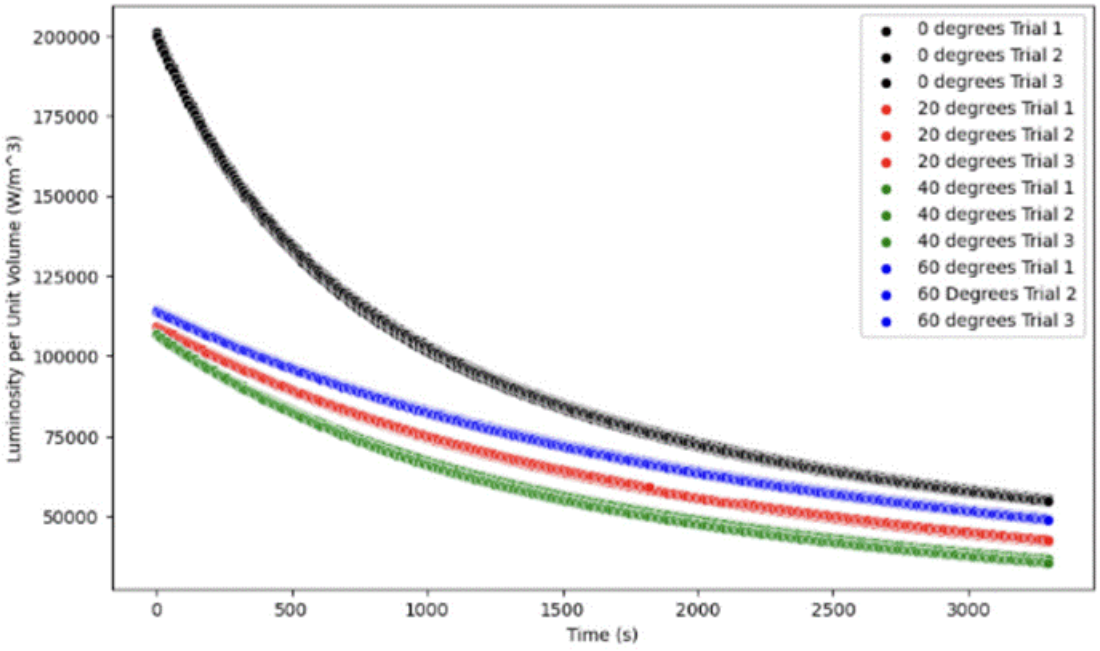

Figure 6. Cooling efficiency of four varies aluminum shells. Luminosity per unit volume versus time for four different shells. All points on Figure 3 were divided by volume to eliminate volume as a variable, providing a more accurate measure of the impact of the surface area on the cooling efficiency (W/m^3). Each point on the graph indicates the energy being emitted by a unit volume per second of the specified shell.

In figure 6, the luminosity was divided by volume to obtain Luminosity per cubic meter versus time. The volume of an object will influence its mass linearly, since the mass is the product of its volume and density. All shells were made with aluminum and thus have the same average

specific heat values of 0.89J/g°C [10]. The amount of energy, in Joules, required to increase the temperature of a shell by one degree can be calculated by multiplying its specific heat and mass. Shells with higher volume and higher mass thus require a larger loss in energy to cool down the same amount compared to other shells. Dividing the luminosity by volume eliminates this difference and allows us to more accurately observe the impact of surface structure and area on cooling.

The results show that the 0° shell significantly outperforms the other shells in cooling efficiency (W/m^3 / second) (Figure 6). This follows the trend observed in Figure 4, where the 60° shell exhibits the second highest cooling efficiency, followed by the 20° then 40° shell. Beyond the measures of temperature, the surface area to volume ratios of each shell was calculated, since both surface area and volume play a key role in cooling [11]. The surface area to volume ratios of the shells show that the 0° shell had a significantly higher ratio compared to the other three, which had similar ratios with each other (Figure 6).

Discussion

The experimental data convey that the flat surface has the highest cooling efficiency, emitting the most Joules per unit volume per second (Figure 6). The thinness of the shell was also most likely important - the 0° shell had the highest surface area to volume ratio of any of the three shells (Table 2). The similarity in surface area to volume ratio could account for the similarity in the cooling rates between the 20°, 40°, and 60° shells (Figure 4). This indicates that the extra shell volume created by the ribs offsets the cooling advantage gained from its increased surface area.

Table 2. Table 2 presents the surface area, volume, surface area (SA) to volume ratio, and mass of the objects positioned at different angles from the horizontal. The angle 0° represents the naked aluminum core, with subsequent shells angled at 20°, 40°, and 60°.

Degrees from the Horizontal	Surface Area (m^2)	Volume (m^3)	SA:V Ratio	Mass (kg)
0°	0.0239	0.0000847	282.1723731	0.228

20°	0.0342	0.000222	154.0540541	0.597
40°	0.0368	0.000244	150.8196721	0.658
60°	0.0462	0.000286	161.5384615	0.772

Since radiation dissipates uniformly in all directions, a point at the center of a ribbed valley emits radiation based on the rib's angle from the horizontal divided by 180°, compared to a point on a flat surface. While a ribbed surface will have a larger surface area and therefore more radiating "points", the overall effectiveness of cooling can be diminished to a point where the increased surface area does not translate to improved cooling.

Smaller increments of the ridge angles were not explored due to financial limitations on the cost of creating multiple aluminum shells. Thus, there could be different results between the 0° and 20° as the smaller ridge heights in the smaller angles may optimize the surface area while not interfering with heat reabsorption [5]. Additionally, higher cooling rates from angles greater than 60° can be expected (Figure 4). Another limitation was the inability to create uniform surface area and volume among the three shells due to manufacturing and monetary restrictions. While this irregularity in the data was compensated by dividing the luminosity by volume (Figure 6), volume and surface area may have a more significant contribution to the object's heat retentivity that has not been explored by this paper. Another limitation of the study was the size of the vacuum chamber used in the experiment. It was observed that the internal temperature of the 5-gallon vacuum chamber was 35°C higher on average than the external room temperature due to the absorption of the heat radiated by the heating apparatus. This may have consistently slowed the cooling rates of the shells.

The results confirm that flatter and smoother surfaces show higher heat radiation rates compared to complex, ridged surfaces. This finding has significant implications for future radiator designs. Flat-surfaced radiators require less time spent machining and thus can be produced at a lower cost, as well as being more portable and foldable. Similarly, spacecraft with smoother exterior can radiate heat more efficiently. Consequently, it becomes crucial to design

spacecraft surfaces with minimal large-angle obstructions to optimize heat dissipation during long distance space missions. As for physical radiator design, large and flat panels will perform the best as they have the highest surface area to volume ratio compared to other shapes.

With the main limitation of this experiment being cost and scalability, future experiments can be improved by ensuring the aluminum radiator blocks have uniform volume and surface area. The heating and cooling process can be improved by using an induction heater to achieve higher temperatures, and by using a larger vacuum chamber to reduce the heat trapping. Other additions could include the careful application of heat-resistant black paint to make the object closer to a perfect blackbody, allowing more accurate usage of the Stefan-Boltzmann law.

One important question is why the 60° shell outperformed both the 40° and 20° shell, and why the 20° shell outperformed the 40° shell. It does not show a clear correlation besides the fact that the 0° shell performed better. Another question to explore could be whether rounder surfaces will perform better compared to flat surfaces.

This study mainly explored whether altering the vertex angle of radiator ribs would enhance cooling efficiency. However, based on the results, the effect of rib angle alone shows a limited impact on radiative transfer. Therefore, a more comprehensive approach will be necessary, incorporating other crucial factors such as high-emissivity materials, thermal coatings, and surface treatments. Materials such as black anodized aluminum and copper oxide are known to have high-emissivity. For instance, black anodized aluminum, commonly used in aerospace applications, has emissivity values as high as 0.85 to 0.90, allowing for higher rates of radiation compared to other surface materials [12,13].

Additionally, thermal coatings can further improve the emissivity of radiators by minimizing the effects of reflective metallic surfaces. Materials such as white ceramic-based coatings and silicon dioxide (SiO_2) are frequently used to enhance thermal radiation. For example, a silicon dioxide coating can achieve emissivity values close to 0.95 [12]. Furthermore, these coatings provide a stable surface that resists degradation in extreme space environments, protecting the radiator from factors like meteoroid impacts and chemical interactions with any residual atmospheric particles.

In contrast, a naked or uncoated radiator typically has a lower emissivity. Uncoated materials such as bare aluminum or titanium may only achieve emissivity values around 0.05 to 0.2, significantly reducing the radiator’s cooling capacity [13]. Thermal coatings, therefore, serve a dual purpose: they increase emissivity while also protecting the radiator surface from the harsh conditions of space. By incorporating these material optimizations alongside the surface geometric configurations, future spacecraft designs can maximize cooling efficiency.

In addition, the aluminum blocks used in this study were heated to a maximum temperature of 477.6 K, significantly lower than the approximate 3000 K that nuclear thermal propulsion systems might reach. While these experimental conditions do not directly emulate the extreme environment of space, they provide a controlled setting in which to observe cooling behavior in near-vacuum conditions and moderate temperatures. These results can still offer insight into the relative effectiveness of angled versus smooth radiator surfaces, though additional studies under more realistic space conditions would be necessary to validate performance at higher temperatures and ultra-low pressures.

Initial hypothesis posited that the smallest rib angle on its surface would yield the highest cooling rate. This proved to be true as the shell with the largest cooling rate was the 0° shell. However, this result is likely due to its high surface area to volume ratio and not necessarily just the surface geometry.

References

[1] Borowski SK, McCurdy DR, Packard TW. Nuclear thermal propulsion (NTP): a proven growth technology for human NEO/Mars exploration missions. 2012 IEEE Aerosp Conf; 2012. https://doi.org/10.1109/aero.2012.6187301.

[2] Oren JA, Howell HR. Space station heat rejection subsystem radiator assembly design and development. SAE Tech Pap Ser; 1995. https://doi.org/10.4271/951651.

[3] Jones RE, Morren WE, Sovey JS, Tacina RR. Space station propulsion. NASA Tech Rep Server. Accessed June 2025. https://ntrs.nasa.gov/api/citations/19880002364/downloads/19880002364.pdf.

[4] Grochalski K, Rukat W, Jakubek B, Wieczorowski M, Słowiński M, Sarbinowska K, et al. The influence of geometry, surface texture, and cooling method on the efficiency of heat dissipation through the heat sink—a review. *Materials*. 2023;16(15):5348. https://doi.org/10.3390/ma16155348.

[5] Kelly F. On Kirchhoff's law and its generalized application to absorption and emission by cavities. 2nd Aerosp Sci Meet; 1965. https://doi.org/10.2514/6.1965-135.

[6] Carter B. *Op amps for everyone*. Burlington (MA): Elsevier Science & Technology Books; 2012.

[7] Gilmore DG. *Spacecraft thermal control handbook, volume I: fundamental technologies*. Reston (VA): American Institute of Aeronautics and Astronautics; 2002. https://doi.org/10.2514/4.989117.

[8] Zielenkiewicz W, Margas E. *Theory of calorimetry*. Berlin: Springer; 2011.

[9] Owocki S. *Fundamentals of astrophysics*. Cambridge: Cambridge Univ Press; 2023.

[10] Buyco EH, Davis FE. Specific heat of aluminum from zero to its melting temperature and beyond. Equation for representation of the specific heat of solids. *J Chem Eng Data*. 1970;15(4):518–523. https://doi.org/10.1021/je60047a035.

[11] Árpád I, Kiss JT, Kocsis D. Role of the volume-specific surface area in heat transfer objects: a critical thinking-based investigation of Newton's law of cooling. *Int J Heat Mass Transf*. 2024;227. https://doi.org/10.2139/ssrn.4583902.

[12] Lu P, Yang T, Gao T. Application of new materials in aerospace thermal management. *Adv Eng Technol Res*. 2023;4(1):50–58. https://doi.org/10.56028/aetr.4.1.50.2023.

[13] Smith FJ, Olson RL. Emissivity coatings for low-temperature space radiators. NASA Tech Rep Server; 1965. https://ntrs.nasa.gov/api/citations/19660006083/downloads/19660006083.pdf.